Multimode δ Sct stars from the Zwicky Transient Facility Survey

Qi Jia[1,2] , Xiaodian Chen[1,2,3,4] , Shu Wang[1,2] , Licai Deng[1,2,3] , Yangping Luo[1] , and Qingquan Jiang[1]
[1] School of Physics and Astronomy, China West Normal University, Nanchong 637009, People's Republic of China; chenxiaodian@nao.cas.cn
[2] CAS Key Laboratory of Optical Astronomy, National Astronomical Observatories, Chinese Academy of Sciences, Beijing 100101, People's Republic of China
[3] School of Astronomy and Space Science, University of the Chinese Academy of Sciences, Beijing 100049, People's Republic of China
[4] Institute for Frontiers in Astronomy and Astrophysics, Beijing Normal University, Beijing 102206, People's Republic of China
Received 2023 December 1; revised 2024 May 15; accepted 2024 May 16; published 2024 June 28

Abstract

We obtain the largest catalog of multimode δ Sct stars in the northern sky to date using the Zwicky Transient Facility (ZTF) Data Release 20. The catalog includes 2254 objects, of which 2181 are new to our study. Among these multimode δ Sct stars, 2142 objects are double-mode δ Sct, while 109 objects are triple-mode δ Sct and three are quadruple-mode δ Sct. By analyzing the light curves in the *r* and *g* bands of the ZTF, we determine the basic parameters of multimode δ Sct stars, including the periods and amplitudes. Periods are checked by comparison with the Optical Gravitational Lensing Experiment catalog of double-mode δ Sct stars. On the Petersen diagram, multimode δ Sct stars form six sequences. We find that in Galactic coordinates, the periods of 1O/F double-mode δ Sct stars at high latitudes are shorter than those of 1O/F double-mode δ Sct stars in the disk, due to metallicity variations. In the future, our catalog can be used to establish the period–luminosity relation and the period–metallicity relation of double-mode δ Sct stars, and to study the Galactic structure.

Unified Astronomy Thesaurus concepts: Periodic variable stars (1213); Pulsating variable stars (1307); Delta Scuti variable stars (370); Stellar oscillations (1617); Distance indicators (394); Astronomy databases (83)

Supporting material: machine-readable tables

1. Introduction

Delta Scuti (δ Sct) stars are pulsating variable stars with periodic variations in brightness (Breger 2000). These stars belong to the Population I stars, while their Population II counterparts are metal poor, classified as SX Phoenecis stars (SX Phe). δ Sct stars have spectral types between A0 and F5, and effective temperatures in the range between 6500 K and 8500 K. The masses of this class of stars range from about $1.5 \leqslant M \leqslant 2.5\,M_\odot$ (Bowman 2017). δ Sct stars exhibit a wide range of pulsation periods, usually between 0.02 and 0.3 days. Their peak-to-peak amplitudes in the visible band (*V* band) can reach approximately 0.9 mag (McNamara 2000a; Balona & Dziembowski 2011; Uytterhoeven et al. 2011; Chang et al. 2013; Bowman 2017). In the Hertzsprung–Russell diagram, δ Sct stars are located in the lower part of the classical Cepheid instability strip and have luminosities ranging from the zero-age main sequence to about 2 mag above the main sequence. These variable stars may also appear in the pre-main-sequence or post-main-sequence phases (Rodríguez & Breger 2001; Dupret et al. 2004; Chang et al. 2013). Such positional variations are due to changes in their evolutionary state and internal structure.

The pulsating phenomenon exhibited by δ Sct stars in their unique evolutionary state provides a rare opportunity to investigate the structure and evolution of these interesting objects (Breger & Pamyatnykh 1998; Murphy et al. 2019). It has been observed that most δ Sct stars have amplitude modulations accompanied by period variations, representing different evolutionary stages (Bowman & Kurtz 2015; Bowman et al. 2016; Bowman 2016). Thus, the identification of

modes of δ Sct stars is an important research focus in asteroseismology (Balona & Evers 1999; Lv et al. 2022; Yang et al. 2022). Mode identification is performed by analyzing the light curves (LCs) of δ Sct stars (Breger et al. 1993). Most δ Sct stars show a nonradial mode while a few high-amplitude δ Sct stars show radial pressure modes (p modes) which are excited by the κ mechanics (Breger 2000). The δ Sct stars usually pulsate simultaneously in more than one mode (Uytterhoeven et al. 2011). Double-mode δ Sct stars are a subtype of δ Sct stars that mainly exhibit two radial pulsation periods, namely the fundamental (F) mode and first-overtone (1O) mode. For most double-mode δ Sct stars, the primary period is longer than the secondary period. There are also a number of double-mode δ Sct stars whose secondary period is in a low-amplitude nonradial mode (Bowman et al. 2016). It is also possible to have three or four radial modes at the same time, which we call triple-mode and quadruple-mode δ Sct (Baglin et al. 1973; Breger 1979, 2000; Petersen & Christensen-Dalsgaard 1996; Balona & Evers 1999; Breger et al. 1999; Rodríguez et al. 2000; Daszyńska-Daszkiewicz et al. 2005). By plotting the relation between the period ratio and the period, also known as the Petersen diagram (Petersen 1973), it is possible to distinguish different double-mode δ Sct stars and to constrain the evolutionary state of double-mode δ Sct stars. Lv et al. (2021, 2022) adopted Kepler data to analyze the periods of two double-mode δ Sct stars.

The period–luminosity relation (PLR) of δ Sct stars is an important tool for measuring cosmic distances. Distances can be estimated by comparing the apparent magnitude with the absolute magnitude determined by the PLR. Recently, Ziaali et al. (2019) and Barac et al. (2022) used parallaxes from Gaia Data Releases 2 and 3 (DR2 and DR3) to derive more accurate PLRs for δ Sct stars. They found that δ Sct stars with higher amplitudes tend to be closer to the ridges of the PLR, while those with lower amplitudes show a more dispersed

distribution. Another study by Jayasinghe et al. ([2020](#)) used Gaia DR2 parallaxes to determine the PLRs of δ Sct stars in the All-Sky Automated Survey for SuperNovae (ASAS-SN) and found a strong correlation between the periods of δ Sct stars and their metallicities. This correlation suggests that the period of δ Sct stars increases as the Galactocentric radius increases, indicating a gradient in metallicity. Moreover, Martínez-Vázquez et al. ([2022](#)) and Gaia Collaboration et al. ([2023](#)) also reported a segmented PLR for extragalactic δ Sct stars. But the fragmentation PLR was denied by the recent PLRs established by Soszyński et al. ([2023](#)) from the Optical Gravitational Lensing Experiment LMC sample.

Over the past two decades, high-cadence optical telescopes have been used to monitor stars. The ground-based telescopes, such as the Zwicky Transient Facility[5] (ZTF; Bellm et al. [2019](#); Graham et al. [2019](#)) and OGLE[6] (Udalski et al. [2015](#)), and the space telescope missions, such as Kepler[7] (Borucki et al. [2010](#); Steffen et al. [2010](#)) and Gaia[8] (Gaia Collaboration et al. [2016](#)) have provided a large amount of high-precision and long-term photometric data for the study of δ Sct stars. Chen et al. ([2020](#)) identified 16,709 δ Sct stars using the ZTF survey, and Jayasinghe et al. ([2020](#)) found 8400 δ Sct stars in ASAS-SN. Pietrukowicz et al. ([2020](#)) and Soszyński et al. ([2021](#)) published a catalog of over 24,000 δ Sct stars based on the OGLE data. Balona & Dziembowski ([2011](#)) analyzed 1568 δ Sct stars using the Kepler data. Gaia detects about 100,000 OBAF-type pulsating stars in the main sequence, of which more than 14,000 are δ Sct stars (Gaia Collaboration et al. [2023](#)).

With the rapid increase of δ Sct stars, it is important to identify multimode δ Sct stars. Chen et al. ([2023](#)) found that the PLR of the double-mode RR Lyrae is not affected by the metallicity, and it is still worth investigating whether this conclusion applies to δ Sct stars. In this work, we search for multimode δ Sct stars based on ZTF DR20. Our data processing and methods are described in Section [2](#). Section [3](#) shows the result of multimode δ Sct stars in ZTF. In Section [4](#), we discuss the statistic properties of 1O/F double-mode δ Sct stars. Section [5](#) summarizes this work.

2. Data and Methods

2.1. ZTF Data

ZTF is a 48 inch Samuel Oschin Schmidt telescope at the Palomar Observatory with a field of view of 47 deg². The main scientific goals are to explore transient phenomena in the Universe, stellar variability, and solar system science (Graham et al. [2019](#); Masci et al. [2019](#)). The ZTF public surveys are divided into two phases, the first of which ran from 2018 March through 2020 September. It obtained photometric measurements in the g and r bands with a three-night cadence in the northern sky and a one-night cadence in the Galactic plane. The uniform exposure time for each observation is 30 s. The second phase, starting in 2020 December, devotes 50% of the available observation time to a two-night cadence photometry in the g and r bands of the northern sky (Bellm et al. [2019](#)).

---

[5] https://www.ztf.caltech.edu/index.html
[6] http://ogle.astrouw.edu.pl
[7] https://archive.stsci.edu/missions-and-data/kepler
[8] https://www.cosmos.esa.int/web/gaia

Based on ZTF DR2 (time span of ~470 days), Chen et al. ([2020](#)) published a catalog with ~780,000 periodic variable stars. We selected 16,709 δ Sct stars from this catalog, and crossmatched them with the ZTF DR20[9] with a radius of $1''$ to obtain the g- and r-band photometry. The mean number of photometry data points in the g and r bands is around 300 and 500, respectively, which is very suitable for discovering multimode δ Sct stars. We searched for multimode δ Sct stars based on g- and r-band LCs.

2.2. Method

We analyzed the periodic signals from the LCs of the two ZTF bands (g and r bands) using the Lomb–Scargle method (Lomb [1976](#); Scargle [1982](#)). This method returns the power spectral density (PSD) over a preset range of frequencies. Since the period of δ Sct stars is very short, we set the minimum and maximum frequencies to 1 day^{-1} and 1000 day^{-1}, respectively. We set the peak oversampling factor to 100 to ensure that each peak is adequately sampled.

We analyzed the raw data and obtained the PSD of each δ Sct star. We recorded the frequency f_1 corresponding to the highest peak in the PSD and used its inverse as the first period P_1 (dominant period). Then based on the first period, we obtained the folded LC and used a sixth-order Fourier series (as in Equation ([1](#))) to fit the LC. The difference between the maximum and minimum values of the fitted line is the amplitude Amp_1 of δ Sct stars. Figure [1](#) is an example of the period determination. The upper panel shows the PSD and folded LC for the first period and the lower panel shows the PSD and folded LC for the second period.

$$m = a_0 + \sum a_i \cos(2\pi it) + \sum b_i \sin(2\pi it) \tag{1}$$

To determine the second-period P_2, we prewhitened the raw data using the fit LC of the first period P_1 to obtain the residual LC. Then the second-period analysis was performed on the residual LC. Similarly, we used the inverse of the frequency f_2 corresponding to the highest peak in the PSD distribution as the second-period P_2 and obtained the amplitude Amp_2 based on the fitted LC. The top panel of Figure [1](#) shows the PSD distribution and folded LC corresponding to the first period, and the bottom panel shows the PSD distribution and folded LC corresponding to the second period. We note that the first period can be longer ($P_1 > P_2$) or shorter ($P_1 < P_2$) than the second period. The long period usually corresponds to F-mode pulsation and the short periods correspond to 1O-, 2O-, or 3O-mode pulsation for δ Sct stars. The PSD significance of the F period may be lower than the PSD significance of the 1O, 2O, or 3O period.

The reliability of the derived periods can be described by the false-alarm probability (FAP). The FAP is a statistical parameter indicating the probability that a random error will be considered as a periodic signal in the absence of a true periodic signal. The FAP was estimated by the maximum PSD value. We excluded multimode δ Sct candidates with FAP values greater than 0.001. In addition, we also required that each candidate has amplitudes (Amp_n) larger than 0.01 mag, which is the lower limit of the accuracy of the ZTF photometry.

We set the automated procedure to continue the prewhitening process on the residual data as long as these two conditions were met (amplitude and FAP), and searched for periods in the

---

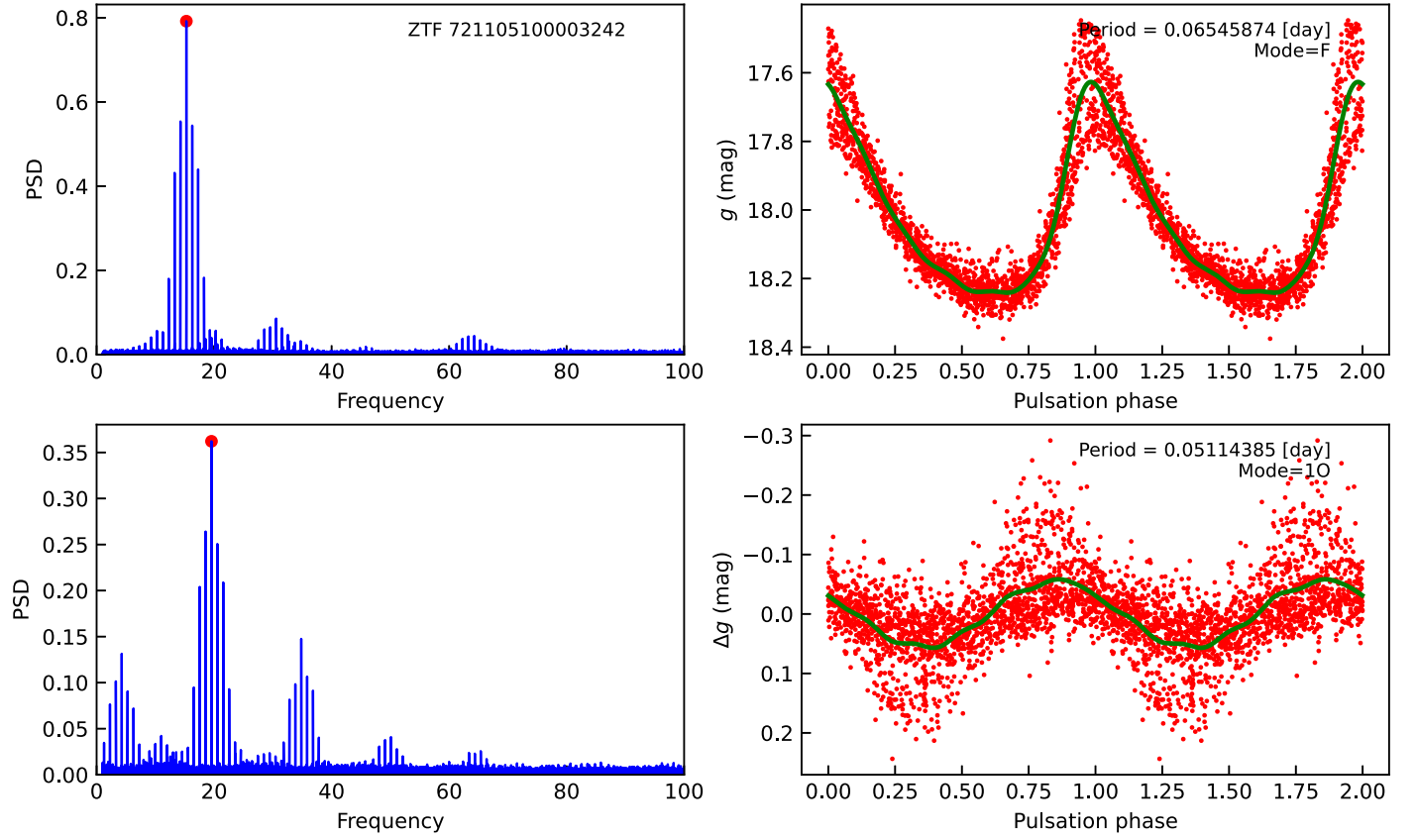[9] https://www.ztf.caltech.edu/ztf-public-releases.html

Figure 1. Example diagram of 1O/F double-mode δ Sct stars for a g-band LC and PSD. Top left: PSD of the original data; the red filled circle shows the maximum PSD. Top right: red dots are the original LC folded by the first period, the green line is the best Fourier fit. Bottom left: PSD of the residual LC after prewhitening; the red filled circle shows the maximum PSD. Bottom right: red dots are the residual LC after prewhitening folded by the second period; the green line is the best Fourier fit to the residual LC.

Table 1
Example of Frequencies Obtained by an Automatic Procedure for 12 δ Sct Stars

ZTF ID	R.A. (J2000)	Decl. (J2000)	f_1	f_2	f_3	f_4	f_5	f_6	Passband
ZTFJ174314.38+181810.6	265.8099413	18.3029559	18.4159	23.5305	23.6314	41.9464	35.216	5.1147	r
ZTFJ174345.66+292526.7	265.9402837	29.4240975	24.0333	30.889	54.9223	6.8557	22.0311	24.0329	r
ZTFJ174623.28+375715.3	266.5970373	37.9542592	17.4586	21.8274	17.8318	39.286	17.7307	4.3688	r
ZTFJ174643.80+285533.4	266.6824994	28.9259522	12.2653	15.7584	28.0238	3.4931	40.2891	8.7722	r
ZTFJ174910.76+531131.0	267.2948619	53.1919563	15.8378	15.8384	15.8374	23.4429	23.4434	23.2144	r
ZTFJ174923.93+152356.3	267.3497535	15.3989847	19.6989	19.9187	25.1866	20.173	39.8719	9.555	r
ZTFJ174945.76+510241.1	267.4401071	51.0447614	15.9293	20.4027	4.4734	36.3321	11.4558	52.2614	r
ZTFJ175110.34+183638.8	267.7931064	18.6107621	19.2241	24.67	24.8255	24.8368	5.446	24.8469	r
ZTFJ175145.87−001058.5	267.9411416	−0.1829098	9.2821	12.0028	21.285	5.7261	17.9839	16.7107	r
ZTFJ175149.33+005540.0	267.955551	0.9277633	9.2299	9.2295	9.2305	9.229	9.2302	16.9963	r
ZTFJ175232.64+101403.5	268.1360574	10.2342752	16.6813	21.3826	4.7013	38.0639	11.98	54.7453	r
ZTFJ175354.56+273625.4	268.4773469	27.6070557	15.4294	19.6585	15.4299	35.0879	4.2291	30.8592	r

Note. ZTF ID: source ID. R.A. and decl.: source position (J2000). $f_1 - f_6$: first to sixth frequencies. Passband: ZTF r passband.

same way. We tried to set the initial number of periods to 16, and by calculation, we found that when more than six periods were obtained, the seventh and onward were combinations frequencies (Pietrukowicz et al. 2013, 2020). Therefore, we set the maximum number of period to six in the later processing. In this step, we obtained 11,003 and 10,588 candidates in the r and g bands, respectively.

Mode classification is a complex task because most of the candidate periods do not correspond to desirable pulsation modes, so we performed the mode classification in two steps (Bowman et al. 2021; Netzel et al. 2022). First, we filtered each

obtained frequency to exclude combination frequencies. We examined all candidate frequencies for δ Sct stars containing multiple frequencies, some of which were cases where the frequencies were added or subtracted, or equal (Kiss et al. 2002; Kurtz et al. 2015). For example, $f_i = a^* f_j + b^* f_e$ where a and b are integers, or zero. We designed an automated procedure to exclude the combination frequencies. In Table 1, we show the six frequencies of some δ Sct stars obtained by our frequency determination procedure, and we can find some combination frequencies. For example, for ZTFJ174345.66 + 292526.7, $f_3 = 1^* f_1 + 1^* f_2$, $f_4 = -1^* f_1 + 1^* f_2$, $f_6 = 1^* f_1$, and f_3, f_4, and f_6
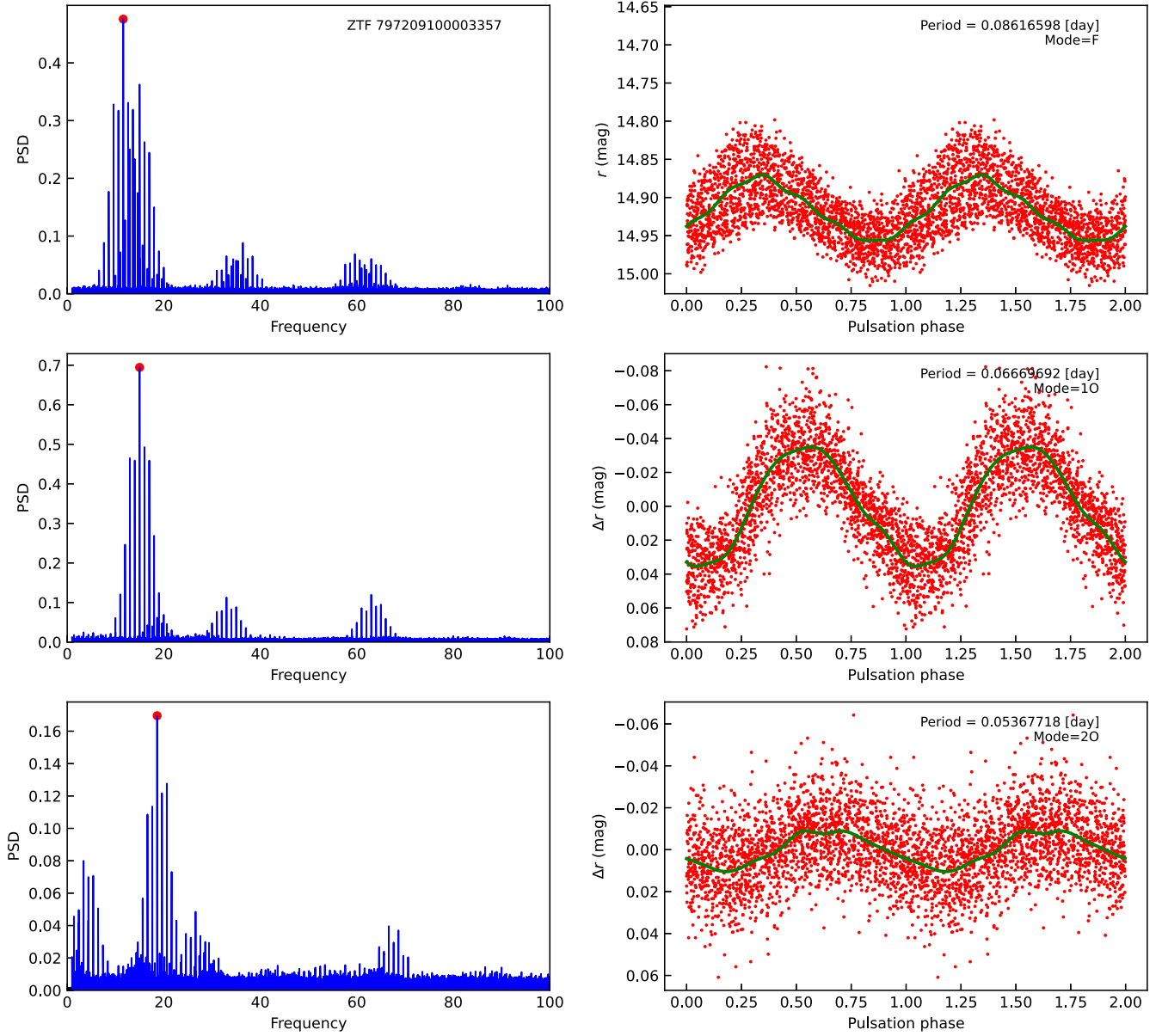
Figure 2. Example diagram of triple-mode 2O/1O/F δ Sct stars for *r*-band LCs (right) and PSDs (left). Top left: PSD of original data with maximum PSD marked in red. Top right: original LC folded by F-mode period (red dots) with the best Fourier fit shown as a green line. Middle left: PSD of residual LC after prewhitening using the period corresponding to the F mode, the maximum PSD marked is in red. Middle right: residual LC folded by 1O-mode period (red dots) with the best Fourier fit shown as a green line. Bottom left: PSD of residual LC after prewhitening using the period corresponding to the 1O mode, the maximum PSD is marked in red. Bottom right: residual LC folded by 2O-mode period (red dots) with the best Fourier fit shown as a green line.

Table 2
Mode Statistics of Multimode δ Sct Stars

Mode	N_{stars}
1O/F	1753
2O/1O	195
3O/2O	96
3O/1O/F	38
2O/1O/F	44
3O/2O/F	9
3O/2O/1O	18
3O/1O	61
3O/F	16
2O/F	21
3O/2O/1O/F	3

are the combination frequencies. Therefore, we retained f_1, f_2, and f_5, which are independent pulsation frequencies. To ensure the accuracy of the procedure of removing combination frequencies, we also calculated the ratio of combination frequencies to independent frequencies and determined that they are not in the usual sequences on the Peterson diagram of multimode δ Sct stars. Then, these combination frequencies were removed.

We refer to the classical period ratios corresponding to each mode pair to help exclude combination frequencies (Breger 2000; Pietrukowicz et al. 2020; Bowman et al. 2021; Soszyński et al. 2021, 2023). We expect the largest number of real frequencies to exist simultaneously. We first screen candidates for the presence of four frequencies, namely F, 1O, 2O, and 3O. If the period ratios are in good agreement, the candidate is labeled as a quadruple-mode δ Sct candidate;
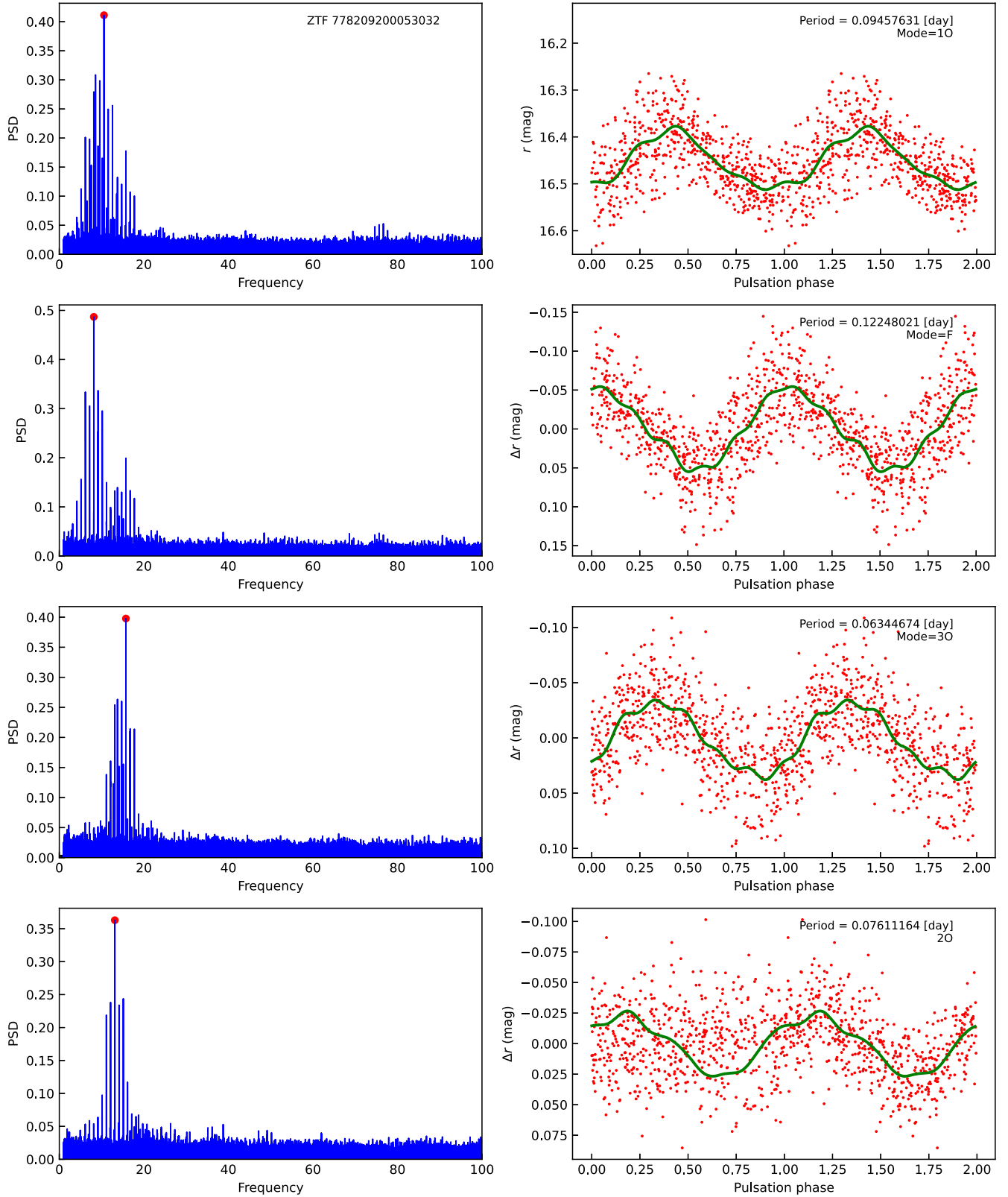
Figure 3. Example diagram of quadruple-mode 3O/2O/1O/F δ Sct stars for *r*-band LCs and PSDs. The left panels show the PSD plots for the corresponding mode period, with the maximum PSD marked in red. The right panels show the LCs folded by the corresponding mode period, with the best Fourier fit line shown in green. The panels correspond to modes 1O, F, 3O, and 2O from top to bottom.

otherwise, it is labeled as a triple-mode δ Sct candidate. Then, the three frequencies are analyzed to determine the corresponding modes. Some frequencies may be missing, e.g., 3O/2O/F. After selecting the triple-mode δ Sct candidates, the remaining ones are the double-mode δ Sct candidates.

After removing the combination periods, we obtained a more reliable sample, with 3890 and 3883 multimode δ Sct
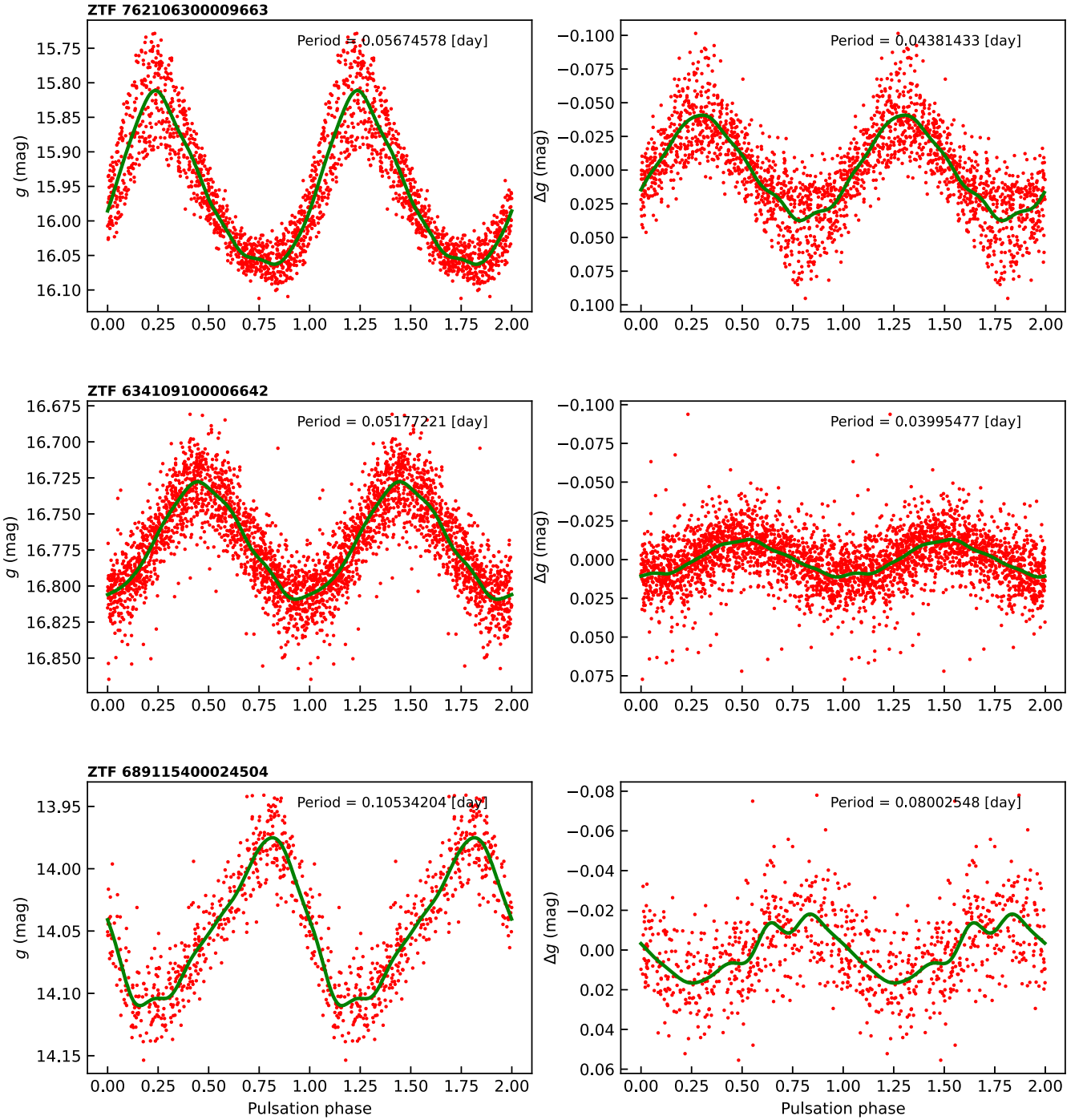
Figure 4. Other examples of g-band LCs. The left panels are the original LCs folded by P_1, and the right panels are the residual LCs after prewhitening folded by P_2.

candidates in the r and g bands, respectively. 677 δ Sct candidates exhibit a triple or quadruple mode while 4460 candidates exhibit a double mode.

In the second step, we perform a more strict selection of modes. Since the 3O and 2O modes have small pulsation amplitudes and the maximum PSD is more susceptible to noise, we performed a more rigorous analysis on samples classified as three or four mode, as well as on the candidates containing a 2O or 3O mode. We calculated the signal-to-noise ratio (S/N) of each maximum PSD by dividing the maximum PSD value by the average PSD value. We required that the PSD S/N of the 2O and 3O candidate periods should be more than 30 and the PSD value should be greater than 0.1 to improve the

reliability of the periods. After screening, we obtained 2182 and 2172 multimode δ Sct candidates in the r and g bands, respectively. We then visually inspected the LC and PSD plots of each candidate and eliminated candidates with multiple strong PSD peaks to further ensure the reliability of each period.

Finally, we obtained 1761 and 1717 multimode δ Sct stars in the r and g bands, respectively. Out of these, 1224 candidates showed reliable periods in both bands. If the number of radial modes identified based on the two bands is different, we suggest using the set of parameters with more modes. If the number of radial modes identified by the two bands is the same, we recommended choosing the set of parameters with the

Table 3
Periods of Triple- and Quadruple-mode δ Sct Stars

ZTF ID	R.A. (J2000)	Decl. (J2000)	F	1O	2O	3O	Passband
ZTFJ002707.80+573740.7	6.7825489	57.6279757	0.1165398	0.0897679	0.0719473	...	g
ZTFJ003240.12+680557.2	8.1672032	68.0992404	0.1640398	0.1301509	...	0.0926695	r
ZTFJ011902.45+561848.4	19.7602403	56.3134413	0.0816329	0.0632725	...	0.0446231	g
ZTFJ015534.52+641251.5	28.8938852	64.2144173	0.1011103	0.0781726	...	0.0553498	g
ZTFJ022719.61+644448.5	36.8317323	64.7468217	...	0.0928653	0.0745411	0.0620484	g
ZTFJ024450.93+515244.9	41.2122211	51.8791557	0.1469574	...	0.0908331	0.0762280	g
ZTFJ041800.37+560842.4	64.5015703	56.1451017	0.1224803	0.0945763	0.0761113	0.0634466	g
ZTFJ051725.58+375800.0	79.3566291	37.966637	0.1206552	0.0931018	0.0748427	...	g
ZTFJ051955.80+330223.5	79.9824919	33.0398638	0.0820884	0.0635637	0.0511918	...	g
ZTFJ053635.83+180016.0	84.1493215	18.0044493	0.0829809	0.0642879	0.0502297	...	g
ZTFJ061454.47+082729.4	93.7269632	8.4581676	0.1043608	0.0805573	...	0.0537804	r
ZTFJ062314.49+132359.1	95.8104118	13.3997492	0.1206204	0.0928877	0.0744759	...	r
ZTFJ064324.79+212736.0	100.8533061	21.4600197	0.1372577	0.1058090	0.0849311	...	g
ZTFJ074121.43+514818.6	115.3393202	51.8051702	0.0515386	0.0400259	...	0.0267000	r
ZTFJ085208.81+475340.8	133.0367432	47.8946839	0.0681228	0.0532180	...	0.0349041	g
ZTFJ094705.64+320154.9	146.7735415	32.0319331	0.1490839	0.1149011	0.0889302	...	g
ZTFJ115725.63+461637.7	179.3568186	46.2770958	0.0565239	0.0442683	0.0363803	...	g
ZTFJ115938.65+283643.5	179.9110739	28.6120961	0.1163245	0.0911218	0.0718774	...	r
ZTFJ160627.43+611815.1	241.6143252	61.3042086	0.0607211	0.0472639	...	0.0312165	r
ZTFJ164334.98+314958.4	250.895759	31.832896	0.0802779	0.0618907	0.0482632	0.0402488	g
ZTFJ165227.35+390102.1	253.1139995	39.0172396	0.0758859	0.0587244	0.0473220	...	g
ZTFJ172627.88+443233.1	261.6162013	44.5425116	0.0517535	0.0402768	...	0.0256526	r
ZTFJ173401.09+320716.7	263.5045805	32.1213193	0.0819214	0.0615111	...	0.0416024	g
ZTFJ181525.21+163047.2	273.8550568	16.5131158	0.0916544	0.0707404	0.0549439	...	g
ZTFJ182458.41+221116.1	276.2434026	22.1878117	0.0773147	0.0605841	...	0.0407111	g
ZTFJ182525.08+123948.6	276.3545401	12.6634854	0.1023325	0.0789146	0.0107359	...	g
ZTFJ182947.45+374500.5	277.4477516	37.7501378	0.1165758	0.0902965	...	0.0635385	g
ZTFJ190853.44+315912.3	287.2227149	31.9867359	0.0942179	0.0728080	0.0583519	...	g
ZTFJ191259.09+141624.4	288.2462314	14.2734536	...	0.1107145	0.1339318	0.1113524	r
ZTFJ192136.47+485114.8	290.4020083	48.8541104	0.0795753	0.0642516	...	0.0422997	g
ZTFJ193545.79+483413.7	293.9408238	48.5704783	0.0954071	0.0748321	0.0603110	...	g
ZTFJ193852.49+391818.7	294.7187579	39.3052037	0.0666380	0.0515842	...	0.0349197	g
ZTFJ193924.92+305249.1	294.853881	30.8802924	0.0923304	0.0713013	0.0572283	...	r
ZTFJ194132.26+115801.8	295.3844368	11.9671693	0.1036147	0.0801730	...	0.0535791	g
ZTFJ194552.24+325957.6	296.4676933	32.9993304	...	0.1986043	0.1586355	0.1332206	r
ZTFJ194552.97+164158.8	296.4707254	16.6996697	0.0815354	0.0640002	0.0520505	...	g
ZTFJ194706.20+363217.0	296.775884	36.5380844	0.1589075	...	0.0947973	0.0780717	r
ZTFJ194926.78+200356.5	297.3616125	20.0656996	0.0923241	0.0709239	0.0595783	...	r
ZTFJ195026.87+445942.1	297.6119672	44.9950402	0.1344034	0.1035363	0.0830579	...	g
ZTFJ195805.05+400049.7	299.5210736	40.0137969	0.1221518	0.0941582	...	0.0607540	r
ZTFJ200045.52+452712.4	300.1897125	45.45344	0.0614813	0.0477953	0.0373422	...	r
ZTFJ200509.43+415657.6	301.2893281	41.9493179	0.1283890	...	0.0821899	0.0689944	g
ZTFJ201154.37+235213.4	302.9765662	23.8703791	0.0944245	0.0755396	0.0609555	...	r
ZTFJ202307.41+113823.2	305.7809105	11.6397825	0.0667728	0.0515535	0.0415349	...	g
ZTFJ173856.54+270327.3	264.735597	27.0575901	0.0746851	0.0566629	...	0.0373380	g
ZTFJ190503.39+162956.8	286.2641608	16.4991235	0.0814394	0.0629045	0.0497054	0.0405029	g
ZTFJ192406.37+264808.3	291.026599	26.8023039	0.1962647	0.1499658	0.1201918	...	g

Notes. ZTF ID: source ID. R.A. and decl.: source position (J2000). F: fundamental period. 1O: first-overtone period. 2O: second-overtone period. 3O: third-overtone period. Passband: ZTF passband. "..." indicates that this mode is not detected.

(This table is available in its entirety in machine-readable form.)

smaller second-period FAP. In total, we obtained a sample of 2254 multimode δ Sct stars. The number counts of each mode are listed in Table 2.

Figure 2 illustrates an example of triple-mode δ Sct stars with a 2O/1O/F mode, and Figure 3 illustrates a quadruple-mode δ Sct star with a 3O/2O/1O/F mode. Figure 4 shows the characteristics of the folded LCs of 1O/F double-mode δ Sct stars. For the first period (left panels), the brightness-ascending phase of most double-mode δ Sct stars takes a shorter time than the brightness-descending phase (top-left panel). For a few double-mode δ Sct stars with low amplitudes, the brightness-

ascending phase takes the same time as the brightness-descending phase (middle-left panel) or longer (bottom-left panel). For the second period (right panels), the amplitude is usually smaller than the first period. LCs for other candidates can be downloaded from China-VO at doi:10.12149/101344.

3. Results

In total, we find 2254 multimode δ Sct, with 2142 double-mode δ Sct, 109 triple-mode δ Sct, and three quadruple-mode δ Sct. Table 3 shows the periods of δ Sct with three or four radial

Table 4
Multimode δ Sct Stars in ZTF DR20

ZTF ID	R.A. (J2000) (deg)	Decl. (J2000) (deg)	P_F^r (days)	PSD_F^r	log FAP_F^r	Amp_F^r (mag)	Amp_{3O}^g (mag)
ZTFJ000013.16+514411.1	0.0548631	51.7364071	0.0698843	0.6049	−137.898	0.046	...
ZTFJ000049.07+551428.0	0.2045118	55.2411286	0.0766785	0.6815	−168.968	0.245	...
ZTFJ000114.74+534305.4	0.3114546	53.7181745	0.0789014	0.5882	−132.138	0.126	...
ZTFJ000123.15+681742.6	0.3464857	68.295184	0.0825984	0.5618	−173.124	0.338	...
ZTFJ000316.54+625516.9	0.8189658	62.9213692	0.1768517	0.0883	−8.366	0.016	...
ZTFJ000406.53+633118.4	1.0272561	63.5217831	...	...	...	...	...
ZTFJ000409.21+570516.3	1.0384164	57.0878665	...	...	...	...	...
ZTFJ000441.51+572904.8	1.1729595	57.4846612	0.0762576	0.8766	−320.000	0.312	...
ZTFJ000442.98+534047.8	1.1791283	53.6799309	...	...	...	...	...
ZTFJ000508.12+571258.9	1.2838952	57.2163783	0.0438734	0.7370	−320.000	0.191	...
ZTFJ000514.81+323303.1	1.3117522	32.5508635	...	...	...	...	...
ZTFJ000536.90+612746.7	1.4037999	61.4629866	...	...	...	...	0.021
ZTFJ000634.49+611228.6	1.6437056	61.2079585	0.0806640	0.7643	−204.250	0.113	...
ZTFJ000639.44+531344.0	1.6643797	53.2288917	...	...	...	...	0.039
ZTFJ000707.20+611036.2	1.7799918	61.1767359	0.0873930	0.5830	−121.751	0.170	...
ZTFJ000850.77+183109.8	2.2115708	18.5193646	0.0752332	0.1866	−22.650	0.028	...
ZTFJ000933.50+562144.3	2.3896312	56.3623363	0.0836583	0.6713	−286.332	0.194	...
ZTFJ001020.14+493126.7	2.5839575	49.5240795	...	...	...	...	...
ZTFJ001023.45+603338.9	2.5977259	60.5608094	0.1718441	0.7759	−199.861	0.082	...
ZTFJ001032.32+322348.0	2.6346907	32.3966982	...	...	...	...	...
ZTFJ001048.18+561927.4	2.7007918	56.3242795	...	...	...	...	0.027
ZTFJ001052.49+563118.6	2.7187621	56.5218396	0.1539481	0.6317	−241.448	0.183	...
ZTFJ001133.52+562739.7	2.8897211	56.4610453	...	...	...	...	0.043
ZTFJ001350.50+500600.3	3.460446	50.1001078	...	...	...	...	...
ZTFJ001424.71+532052.6	3.6030072	53.3479601	0.0859501	0.9102	−320.000	0.252	...
ZTFJ001452.28+595603.4	3.7178555	59.9342835	...	...	...	...	0.076
ZTFJ001454.08+705311.7	3.725387	70.8866208	0.0787709	0.8523	−221.559	0.212	...
ZTFJ001508.70+434022.1	3.7862786	43.672824	0.0707618	0.6352	−170.469	0.396	...
ZTFJ001616.57+122320.5	4.0690587	12.3890231	0.0490582	0.8905	−241.631	0.285	...
ZTFJ001737.44+613711.4	4.4060306	61.6198361	...	...	...	...	...
ZTFJ001825.64+670205.9	4.6068601	67.034985	0.0733460	0.7245	−161.080	0.135	...
ZTFJ001958.76+460858.8	4.9948454	46.1496626	0.0591786	0.8123	−88.713	0.329	...
ZTFJ002132.58+182817.4	5.3857876	18.4715083	0.0653385	0.2477	−35.938	0.112	...
ZTFJ002331.41+713953.2	5.8809224	71.6647767	0.0820087	0.7447	−165.862	0.127	...
ZTFJ002345.17+644554.8	5.9382365	64.7652377	0.1097914	0.5831	−111.574	0.097	...
ZTFJ002507.56+632931.9	6.2815526	63.4922072	...	...	...	...	...
ZTFJ002622.93+562517.2	6.5955714	56.4214408	0.0723140	0.7183	−182.121	0.213	...
ZTFJ002707.80+573740.7	6.7825467	57.6279743	0.1165400	0.4041	−72.155	0.052	...
ZTFJ002725.50+371018.8	6.8562575	37.1718835	0.0527894	0.6876	−200.862	0.182	...
ZTFJ002843.66+642637.2	7.1819293	64.4436954	0.0807416	0.2081	−27.366	0.047	...
ZTFJ002928.84+541842.6	7.3702144	54.311838	0.0620472	0.8251	−271.473	0.236	...
ZTFJ005008.94+411040.4	12.5372821	41.177881	0.0554433	0.5507	−165.096	0.180	...

Notes. Mag_F^r, P_F^r, PSD_F^r, log FAP_F^r, Amp_F^r: mean magnitude, period, maximum power spectral density, false-alarm probability, and amplitude corresponding to the F mode in ZTF r band. P_{1O}^r, PSD_{1O}^r, log FAP_{1O}^r, Amp_{1O}^r: period, maximum power spectral density, false-alarm probability, and amplitude corresponding to the 1O mode in ZTF r band. P_{2O}^r, PSD_{2O}^r, log FAP_{2O}^r, Amp_{2O}^r: period, maximum power spectral density, false-alarm probability, and amplitude corresponding to the 2O mode in ZTF r band. P_{3O}^r, PSD_{3O}^r, log FAP_{3O}^r, Amp_{3O}^r: period, maximum power spectral density, false-alarm probability, and amplitude corresponding to the 3O mode in ZTF r band. "..." indicates that this mode is not detected.

(This table is available in its entirety in machine-readable form.)

modes, with columns (4)–(7) showing the periods of the F, 1O, 2O, and 3O modes, respectively. The last column records the band used to obtain these periods.

Table 4 lists the parameters of 2254 multimode δ Sct stars. These parameters include position, period of each mode, and the corresponding PSD, FAP, and amplitude, with a null value indicating that the mode has not been detected. The machine-readable version of this table also includes the individual parameters measured in the g and r bands.

The F mode has a maximum period of 0.29088 day, a minimum period of 0.04 day, and an average value of 0.08171 day. For the 1O mode, the maximum, minimum, and average

periods are 0.22346 day, 0.03217 day, and 0.06765 day, respectively. The 2O mode has maximum and minimum periods of 0.18946 day and 0.03046 day, and an average value of 0.08842 day. The 3O mode has maximum and minimum periods of 0.15931 day and 0.02367 day, and an average value of 0.07118 day. More discussion on the statistical properties about the 1O/F of these parameters is in Section 4.

To better evaluate the confidence of our sample, we crossmatched it with the OGLE catalog, which includes 4023 and 1838 double-mode δ Sct stars in the Galactic bulge and the Galactic southern disk, respectively (Pietrukowicz et al. 2020). We found that 73 multimode δ Sct stars were included in

Table 5
Comparison of the First Periods and Second Periods of Multimode δ Sct Stars Determined by Our Catalog and the OGLE Catalog

ZTF ID	R.A. (J2000) (deg)	Decl. (J2000) (deg)	OGLE P_1 (days)	ZTF P_1 (days)	OGLE P_2 (days)	ZTF P_2 (days)
ZTFJ054655.19+155908.3	86.72996	15.98564	0.08503635	0.0850360	0.0659124	0.0659121
ZTFJ060440.42+083432.3	91.16845	8.57566	0.07191587	0.0719158	0.04854491	0.0485444
ZTFJ061355.52+034318.0	93.48134	3.72168	0.08596043	0.0859603	0.06677114	0.0667712
ZTFJ062413.66+050418.0	96.05695	5.07169	0.15025444	0.1502542	0.1155531	0.1155533
ZTFJ062547.82+191921.0	96.44928	19.3225	0.1413627	0.1413625	0.10852826	0.1085282
ZTFJ062552.25-005202.6	96.46774	−0.86739	0.08598725	0.0859880	0.06667738	0.0666785
ZTFJ062824.41+035852.5	97.10174	3.98126	0.14158798	0.1415881	0.12732041	0.112906[b]
ZTFJ063629.09-051433.9	99.12124	−5.24276	0.138682	0.1386829	0.18032694	0.1803272
ZTFJ063753.01-033949.7	99.4709	−3.66383	0.13108672	0.1310867	0.10104135	0.1010403
ZTFJ064304.96+080714.7	100.77068	8.12076	0.13705798	0.1370576	0.10903951	0.1090399
ZTFJ064320.31+060135.4	100.83463	6.02651	0.1174762	0.1174762	0.09772504	0.0977247
ZTFJ064717.99+061003.3	101.82499	6.16759	0.12671519	0.1267154	0.14258489	0.1030856[b]
ZTFJ065247.18-090306.6	103.19659	−9.05185	0.09385503	0.0938550	0.07268911	0.0726892
ZTFJ065350.50-130017.1	103.46042	−13.00477	0.14432489	0.1443258	0.12594376	0.1118607[b]
ZTFJ065407.53+050434.3	103.53141	5.07622	0.10114655	0.1011467	0.07807166	0.0780718
ZTFJ065704.42-083331.2	104.26843	−8.55868	0.12992842	0.1299283	0.09998667	0.0999870
ZTFJ065818.31-021908.2	104.57632	−2.31895	0.09357905	0.0935790	0.07247291	0.0724733
ZTFJ184116.17-115906.6	280.31739	−11.98518	0.06057093	0.0605708	0.04689278	0.0468926
ZTFJ184333.95+044143.6	280.89147	4.69546	0.04798205	0.0619148	0.06191417	0.0479824[a]
ZTFJ184532.70+092424.2	281.38628	9.40673	0.06176577	0.0617659	0.04775663	0.0477563
ZTFJ184607.72+124928.0	281.53219	12.82445	0.06448798	0.0644882	0.04999730	0.0499978
ZTFJ184807.47-054828.5	282.03113	−5.80794	0.08144335	0.0814431	0.06462169	0.0646215
ZTFJ184837.05+123057.7	282.15439	12.51604	0.10062764	0.0776992	0.07769838	0.1006291[a]
ZTFJ185121.24+004235.4	282.83851	0.70986	0.09587564	0.0958755	0.07404729	0.0740473
ZTFJ185336.75-034220.8	283.40313	−3.70578	0.07366549	0.0736642	0.09469556	0.0946936
ZTFJ185452.44-052428.0	283.71852	−5.40778	0.18920317	0.1892029	0.14466831	0.1446693
ZTFJ190543.74-052401.3	286.43229	−5.40037	0.07401666	0.0740168	0.05715781	0.0571581
ZTFJ190620.59+145937.3	286.58582	14.99372	0.08148242	0.0814825	0.06303693	0.0630369
ZTFJ190704.49-000737.3	286.76875	−0.12705	0.07215581	0.0721557	0.05586513	0.0558649
ZTFJ190850.13+010116.0	287.20889	1.02112	0.08203788	0.0820377	0.06394150	0.0639415
ZTFJ191229.13-030916.9	288.1214	−3.15472	0.08440821	0.0844081	0.07011598	0.0655097[b]
ZTFJ191306.40+210539.4	288.27669	21.09428	0.14697661	0.1469794	0.11429987	0.1142993

Notes. OGLE P_1, ZTF P_1: first periods determined by OGLE and ZTF DR20 data. OGLE P_2, ZTF P_2: second periods determined by OGLE and ZTF DR20 data.
[a] ZTF P_1 is equal to OGLE P_2 and ZTF P_2 is equals OGLE P_1.
[b] Objects with similar P_1 but different P_2.

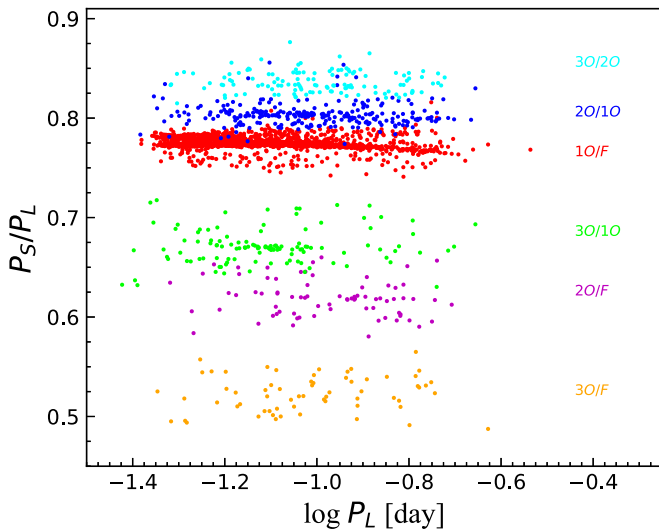(This table is available in its entirety in machine-readable form.)

Figure 5. Petersen diagram of multimode δ Sct stars. The period ratio (*y*-axis) is the short period (P_S) divided by the long period (P_L).
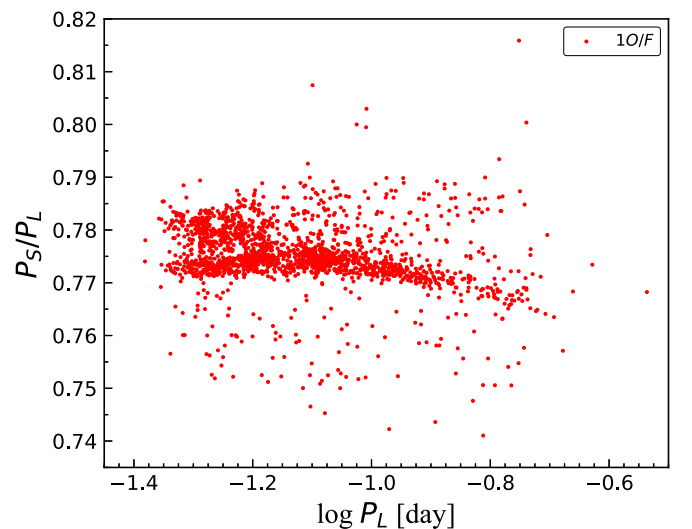
Figure 6. Petersen diagram of 1O/F double-mode δ Sct stars. The period ratio (*y*-axis) is the 1O-mode period divided by the F-mode period.
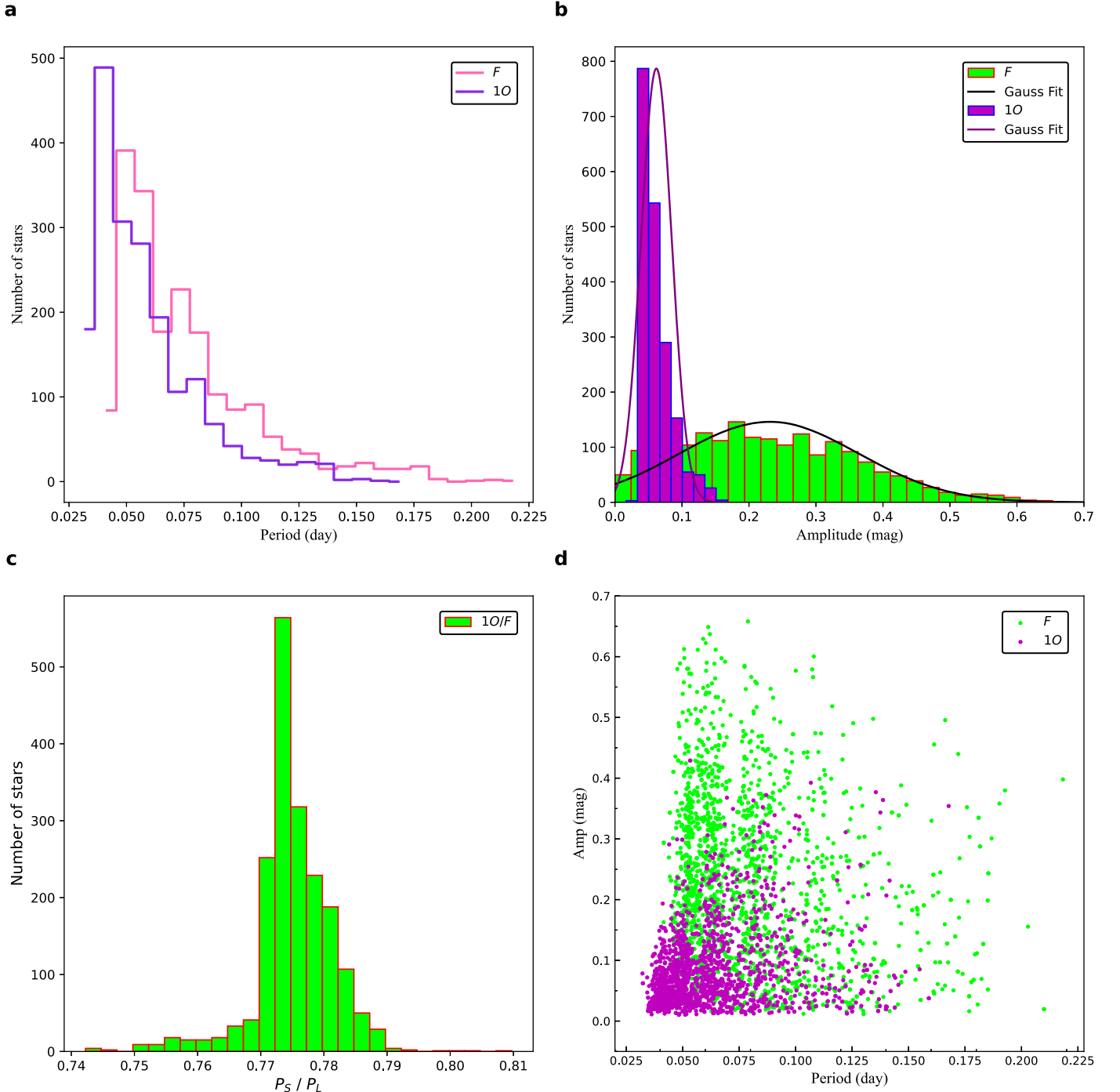
a

b

c

d

Figure 7. Statistical properties of the 1O/F double-mode δ Sct stars. (a) Histograms of the F-mode period and 1O-mode period. (b) Histograms of the amplitude corresponding to the F and 1O modes; the two solid lines are the Gaussian fits. (c) Histograms of the period ratio. (d) Distribution of amplitude vs. period.

OGLE's catalog (see Table 5). The majority of them are in 1O/F mode, and a few are in other modes. By comparing the first periods P_1 determined by ZTF and OGLE data, we found that 71 δ Sct stars are consistent, if we considered that the period difference is not greater than 0.00001. For the other two δ Sct stars, our two periods are just the opposite of the two periods determined by OGLE (see Table 5, labeled [a]). That is, ZTF $P_1 = $ OGLE P_2 and ZTF $P_2 = $ OGLE P_1. For both of them, the amplitudes and maximum PSDs of their two periods are relatively close to each other, and the strongest period may alternate in different ephemerides (HJD$_{OGLE}$ < 2458762,

HJD$_{ZTF}$ > 2458205). For the second-period P_2, the period differences of 69 δ Sct stars are less than 0.0001. Four δ Sct stars show differences on the P_2 (see Table 5, labeled [b]). For these four, OGLE's period ratio is significantly deviated from 0.77, and their second period is likely the other mode or an aliased period.

Overall, the average proportion of our two periods that agree with the OGLE periods is 95.8%. Considering that the second period of δ Sct stars is more difficult to identify than that of RR Lyrae, this proportion shows that our sample of multimode δ Sct stars is reliable.

(a)

(b)
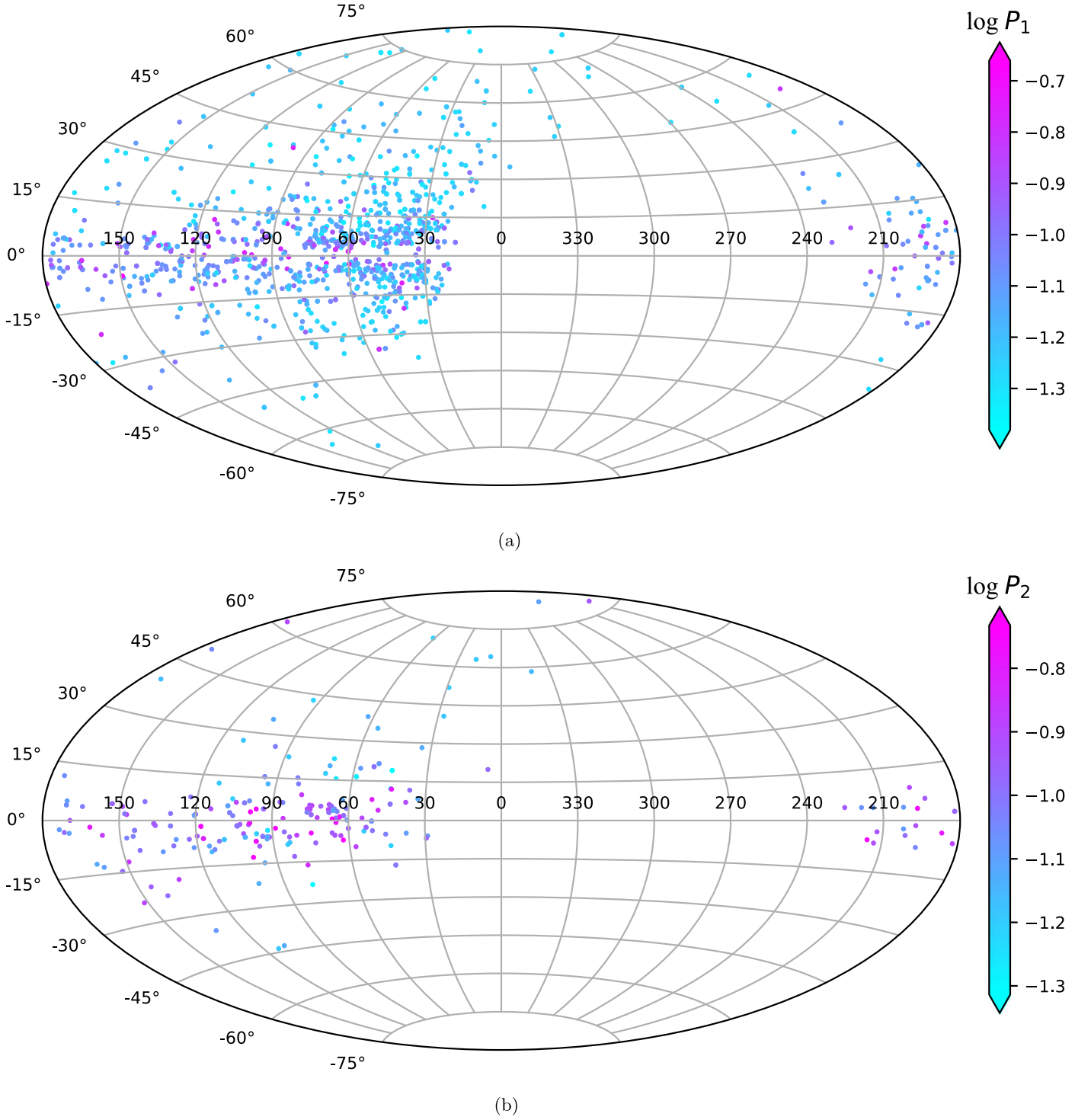
Figure 8. All-sky distribution of 1O/F double-mode δ Sct stars in Galactic coordinates. The top panel shows the sample with $P_1 > P_2$, while the bottom panel shows the sample with $P_1 < P_2$. The colors indicate the logarithm of the longer period P_L.

4. Discussion

The Petersen diagram of multimode δ Sct stars is shown in Figure 5. P_S/P_L represents the ratio of the shorter and longer periods, and $\log(P_L)$ is the logarithm of the longer periods. Different colored dots show different modes: red dots indicate the 1O/F mode, blue dots indicate the 1O/2O mode, cyan dots indicate the 3O/2O mode, green dots indicate the 3O/1O mode, magenta dots indicate the 2O/F mode, and orange dots indicate the 3O/F mode. It is worth noting that there may be mixing between different modes on the Peterson diagram. For a δ Sct star, when only two periods are detected, we classify them by strict ranges of period ratios. At this point there will be a small number of δ Sct stars that are misclassified, such as the modes of 1O/F and 2O/1O. When there are three or four periods detected, we can classify the modes by multiple sets of period ratios, and the classification accuracy will be higher.

Multimode δ Sct stars can be used to obtain stellar masses and luminosities, and can also be used as a good distance tracer. Here, we focus on discussing the statistical properties of 1O/F-mode δ Sct stars, which account for the majority of multiperiod δ Sct stars. We draw their Petersen diagram separately in Figure 6. On this diagram, we can see a distinct sequence with period ratios ranging from 0.760 to 0.775 (McNamara 2000b; Breger 2000) and a clump with a period ratio around 0.78. This clump was also found by Soszyński et al. (2021). According to Breger (2000), the sequence corresponds to Population I δ Sct stars, while the clump is likely formed by Population II SX Phe stars. We found that the amplitude and amplitude ratio distribution of the clump and the sequence is similar.

Figure 7(a) shows the histograms of the F (green) and 1O (magenta) mode period for 1O/F double-mode δ Sct stars. We can see that the distribution of the two periods is similar, with most of them being less than 0.6 days. Figure 7(b) shows the histograms of the amplitude, and we performed a Gaussian fit to the histograms (two solid curves). For F and 1O modes, μ are 0.230 mag and 0.062 mag, while σ are 0.133 mag and 0.023 mag, respectively. For δ Sct stars with a 1O mode, their amplitudes are smaller than 0.2 mag, which is significantly smaller than that of the F mode. Figure 7(c) is the histogram of the period ratios. It is clear that the period ratios of δ Sct stars are almost concentrated between 0.75 and 0.79 with a peak at about 0.774. Figure 7(d) shows the distribution of amplitude versus period; the amplitude of the 1O mode is smaller than that of the F mode.

Figure 8 shows the all-sky distribution of these 1O/F double-mode δ Sct stars in Galactic coordinates. We divided them into two samples: the first period is the F mode and the second period is the F mode. These two samples represent F-mode PSDs that are greater or less than 1O-mode PSDs, respectively. The colors show the logarithm of the longer period P_L. We find that the period increases from the high latitude to the Galactic plane for the two samples, which was also found by Soszyński et al. (2021). This trend of period distribution is caused by the difference in metallicities, and the mean pulsation period of the metal-poor δ Sct stars is shorter than those of the metal-rich δ Sct stars (Jayasinghe et al. 2020).

5. Conclusion

We designed procedures to obtain periods and exclude combination periods based on δ Sct stars' LCs and residual LCs. Then, we obtained a sample of 2254 multimode δ Sct stars based on ZTF DR20, of which 2181 are newly discovered. This is the largest sample in the northern sky. For 1761 and 1717 multimode δ Sct stars, we determined the g- and r-band periods, pulsation mode, amplitudes, and the FAPs of the periods, respectively. Double-mode δ Sct stars comprise 2142 objects, while 109 objects are triple-mode δ Sct and three are quadruple-mode δ Sct.

Different multimode δ Sct stars have different distributions on the Petersen diagram, among which we focused on the 1O/F double-modal δ Sct stars. They are presented as a sequence and a clump at the short-period end on the Petersen diagram. In Galactic coordinates, the period of 1O/F double-mode δ Sct stars at high latitudes is shorter than that on the disk, which is caused by different metallicities. Short-period double-mode δ Sct stars have lower metallicities. In the future, this sample of 1O/F double-mode δ Sct stars will help us to better understand the internal structure and evolutionary history of δ Sct stars, as well as to constrain their masses. Double-mode δ Sct stars can be used as standard candles to measure distances to clusters and dwarf galaxies, and can also be used to study the structure and evolution of the Milky Way.

ORCID iDs

Qi Jia ⬡ https://orcid.org/0000-0002-0786-7307
Xiaodian Chen ⬡ https://orcid.org/0000-0001-7084-0484
Shu Wang ⬡ https://orcid.org/0000-0003-4489-9794
Licai Deng ⬡ https://orcid.org/0000-0001-9073-9914
Yangping Luo ⬡ https://orcid.org/0000-0003-3736-6076

References

Baglin, A., Breger, M., Chevalier, C., et al. 1973, A&A, 23, 221
Balona, L. A., & Dziembowski, W. A. 2011, MNRAS, 417, 591
Balona, L. A., & Evers, E. A. 1999, MNRAS, 302, 349
Barac, N., Bedding, T. R., Murphy, S. J., & Hey, D. R. 2022, MNRAS, 516, 2080
Bellm, E. C., Kulkarni, S. R., Graham, M. J., et al. 2019, PASP, 131, 018002
Borucki, W. J., Koch, D., Basri, G., et al. 2010, Sci, 327, 977
Bowman, D. M. 2016, PhD thesis, Univ. of Central Lancashire
Bowman, D. M., Hermans, J., Daszyńska-Daszkiewicz, J., et al. 2021, MNRAS, 504, 4039
Bowman, D. M., & Kurtz, D. W. 2015, EPJWC, 101, 06013
Bowman, D. M., Kurtz, D. W., Breger, M., Murphy, S. J., & Holdsworth, D. L. 2016, MNRAS, 460, 1970
Bowman, D. M. 2017, Amplitude Modulation of Pulsation Modes in Delta Scuti Stars (Cham: Springer)
Breger, M. 1979, PASP, 91, 5
Breger, M. 2000, in ASP Conf. Ser. 210, Delta Scuti and Related Stars, ed. M. Breger & M. Montgomery (San Francisco, CA: ASP), 3
Breger, M., & Pamyatnykh, A. A. 1998, A&A, 332, 958
Breger, M., Pamyatnykh, A. A., Pikall, H., & Garrido, R. 1999, A&A, 341, 151
Breger, M., Stich, J., Garrido, R., et al. 1993, A&A, 271, 482
Chang, S. W., Protopapas, P., Kim, D. W., & Byun, Y. I. 2013, AJ, 145, 132

Chen, X., Wang, S., Deng, L., et al. 2020, ApJS, 249, 18
Chen, X., Zhang, J., Wang, S., & Deng, L. 2023, NatAs, 7, 1081
Daszyńska-Daszkiewicz, J., Dziembowski, W. A., Pamyatnykh, A. A., et al. 2005, A&A, 438, 653
Dupret, M. A., Grigahcène, A., Garrido, R., Gabriel, M., & Scuflaire, R. 2004, A&A, 414, L17
Gaia Collaboration, De Ridder, J., Ripepi, V., et al. 2023, A&A, 674, A36
Gaia Collaboration, Prusti, T., de Bruijne, J. H. J., et al. 2016, A&A, 595, A1
Graham, M. J., Kulkarni, S. R., Bellm, E. C., et al. 2019, PASP, 131, 078001
Jayasinghe, T., Stanek, K. Z., Kochanek, C. S., et al. 2020, MNRAS, 493, 4186
Kiss, L. L., Derekas, A., Alfaro, E. J., et al. 2002, A&A, 394, 97
Kurtz, D. W., Shibahashi, H., Murphy, S. J., Bedding, T. R., & Bowman, D. M. 2015, MNRAS, 450, 3015
Lomb, N. R. 1976, Ap&SS, 39, 447
Lv, C., Esamdin, A., Pascual-Granado, J., Hernández, A. G., & Hasanzadeh, A. 2022, AJ, 164, 218
Lv, C., Esamdin, A., Zeng, X., et al. 2021, AJ, 162, 48
Martínez-Vázquez, C. E., Salinas, R., Vivas, A. K., & Catelan, M. 2022, ApJL, 940, L25
Masci, F. J., Laher, R. R., Rusholme, B., et al. 2019, PASP, 131, 018003
McNamara, D. H. 2000a, in ASP Conf. Ser. 210, Delta Scuti and Related Stars, ed. M. Breger & M. Montgomery (San Francisco, CA: ASP), 373

McNamara, D. H. 2000b, PASP, 112, 1096
Murphy, S. J., Hey, D., Van Reeth, T., & Bedding, T. R. 2019, MNRAS, 485, 2380
Netzel, H., Pietrukowicz, P., Soszyński, I., & Wrona, M. 2022, MNRAS, 510, 1748
Petersen, J. O. 1973, A&A, 27, 89
Petersen, J. O., & Christensen-Dalsgaard, J. 1996, A&A, 312, 463
Pietrukowicz, P., Dziembowski, W. A., Mróz, P., et al. 2013, AcA, 63, 379
Pietrukowicz, P., Soszyński, I., Netzel, H., et al. 2020, AcA, 70, 241
Rodríguez, E., & Breger, M. 2001, A&A, 366, 178
Rodríguez, E., López-González, M. J., & López de Coca, P. 2000, A&AS, 144, 469
Scargle, J. D. 1982, ApJ, 263, 835
Soszyński, I., Pietrukowicz, P., Skowron, J., et al. 2021, AcA, 71, 189
Soszyński, I., Pietrukowicz, P., Udalski, A., et al. 2023, AcA, 73, 105
Steffen, J. H., Batalha, N. M., Borucki, W. J., et al. 2010, ApJ, 725, 1226
Udalski, A., Szymański, M. K., & Szymański, G. 2015, AcA, 65, 1
Uytterhoeven, K., Moya, A., Grigahcène, A., et al. 2011, A&A, 534, A125
Yang, T.-Z., Zuo, Z.-Y., Sun, X.-Y., Tang, R.-X., & Esamdin, A. 2022, ApJ, 936, 48
Ziaali, E., Bedding, T. R., Murphy, S. J., Van Reeth, T., & Hey, D. R. 2019, MNRAS, 486, 4348